NANO LETTERS

Letter

pubs.acs.org/NanoLett

Tailoring the Electronic Structure in Bilayer Molybdenum Disulfide via Interlayer Twist

Arend M. van der Zande,[†,‡,*] Jens Kunstmann,[†,§] Alexey Chernikov,[∥] Daniel A. Chenet,[‡] YuMeng You,[∥] XiaoXiao Zhang,[∥] Pinshane Y. Huang,[⊥] Timothy C. Berkelbach,[†,§] Lei Wang,[‡] Fan Zhang,[‡] Mark S. Hybertsen,[†,#] David A. Muller,[⊥,¶] David R. Reichman,[†,∥] Tony F. Heinz,[†,∥] and James C. Hone[†,‡]

[†]Energy Frontier Research Center, [‡]Department of Mechanical Engineering, [§]Department of Chemistry, and [∥]Departments of Physics and Electrical Engineering, Columbia University, New York, New York 10027, United States

[⊥]School of Applied and Engineering Physics, Cornell University, Ithaca, New York 14853, United States

[#]Center for Functional Nanomaterials, Brookhaven National Laboratory, Upton, New York 11973, United States

[¶]Kavli Institute at Cornell for Nanoscale Science, Ithaca, New York 14853, United States

Supporting Information

ABSTRACT: Molybdenum disulfide bilayers with well-defined interlayer twist angle were constructed by stacking single-crystal monolayers. Varying interlayer twist angle results in strong tuning of the indirect optical transition energy and second-harmonic generation and weak tuning of direct optical transition energies and Raman mode frequencies. Electronic structure calculations show the interlayer separation changes with twist due to repulsion between sulfur atoms, resulting in shifts of the indirect optical transition energies. These results show that interlayer alignment is a crucial variable in tailoring the properties of two-dimensional heterostructures.

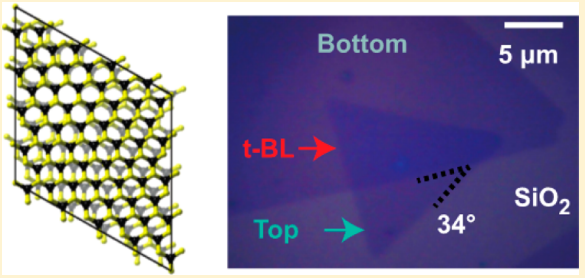

KEYWORDS: *Molybdenum disulfide, twisted bilayer, heterostructure, interlayer interaction, band structure*

A unique feature of two-dimensional (2D) van der Waals layered materials like graphene, hexagonal boron nitride, and the transition metal dichalcogenides (TMDs) is the possibility to form high-quality homo- or heterojunction interfaces without restrictions of lattice matching or even interlayer crystallographic alignment. This new class of atomically thin materials has potential applications including field-effect transistors,[1−4] memory cells,[5] integrated circuits,[2,6] tunnel junctions,[7] photosensors,[8] and photovoltaics.[9,10] In addition to their interesting properties as isolated 2D layers, these ultrathin materials are sensitive to environmental and interlayer interactions, and understanding these interactions is a key scientific challenge for building functional heterojunction devices and novel hybrid 2D materials. Substrate effects can, for example, strongly influence charge transport properties in graphene,[11] while combinations of nonaligned (or twisted) 2D materials, such as twisted-bilayer (t-BL) graphene[12−14] or graphene/hexagonal boron nitride interfaces,[15,16] exhibit distinctive changes to their optical and electronic properties induced by their interactions.

Transition metal dichalcogenide crystals including MoS_2, $MoSe_2$, WS_2, and WSe_2 can be prepared as atomically thin semiconductors. Their electronic, optical,[17,18] and vibrational properties[19] are also known to be significantly modified by interlayer interactions. Most strikingly, crystalline layers of these TMDs are direct gap semiconductors in their monolayer form but exhibit an indirect gap as bilayer and thicker samples. To date, however, interlayer interaction has only been studied in the case of crystallographically aligned layers, as found in samples exfoliated from bulk materials.[17−19] Recently, there has also been a surge of interest in heterojunctions of monolayer TMDs.[20−23] In most of these heterojunctions, the layers are usually arbitrarily aligned with respect to each other leading to a twisted, incommensurate crystal structure. Therefore, there is strong motivation to understand how twist affects interlayer interactions in TMDs and other layered materials.

In this work, we examine both experimentally and theoretically the influence of interlayer twist angle on the optical and vibrational properties of MoS_2 bilayers. t-BLs are prepared by mechanically stacking two crystalline monolayers and their symmetry and stacking angle are confirmed by optical second harmonic generation. Despite the incommensurate structure, we observe significant effects of interlayer interaction. Most notably, the indirect-gap character of the t-BL is maintained for all twist angles. In this respect, t-BL MoS_2 more closely resembles crystallographic bilayer MoS_2 than it does two weakly perturbed direct-gap monolayers. Moreover, varying the twist angle significantly tunes the indirect gap, but

Received: March 21, 2014
Revised: May 21, 2014
Published: June 16, 2014

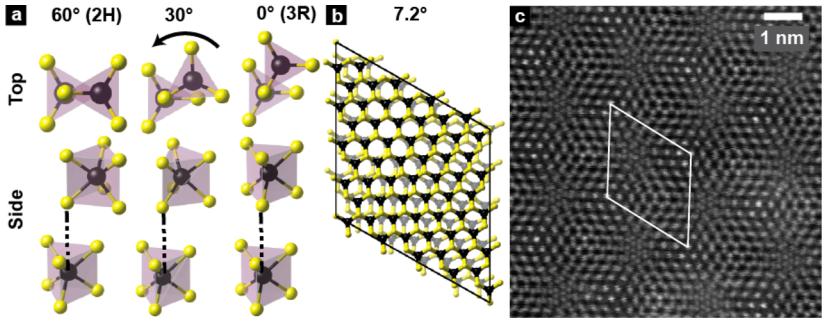

Figure 1. (a) Top and side views of the crystal alignment of bilayer MoS_2 with twist angles of 60° (2H phase), 30°, and 0° (3R phase). (b) Diagram of a unit cell for a 7.2° twisted bilayer. The bottom layer is shaded gray for clarity. (c) High resolution ADF-STEM image of a bilayer with a twist angle of 8.5° and a moiré quasi-periodicity of 2.5 nm. A unit cell is highlighted in white.

only weakly tunes the direct gap. We explain this behavior in terms of the character of the wave functions in different parts of the Brillouin zone and changes in the interlayer spacing of the relaxed structures with twist angle. We also report the relatively subtle changes to the phonon structure of the materials that is observed in the Raman response in t-BL samples. Taken together, these measurements and the associated theoretical treatment lead not only to deeper understanding of the nature of interlayer interactions but also show that twist can be used as a parameter to tune key electronic properties of the material.

Figure 1a depicts the structure of bilayer MoS_2 for different twist angles θ. At $\theta = 0°$, the hexagons in each layer are aligned, whereas at $\theta = 60°$ (or, equivalently, $\theta = 180°$), they are antialigned. Importantly, the layers are antialigned in the most abundant 2H-phase of bulk MoS_2 and are aligned in the rarer 3R bulk phase. Most measurements on exfoliated bilayers to date have been performed on the 2H phase material. For arbitrary twist angles, the MoS_2 bilayers form repeating moiré patterns with a quasi periodicity that depends on θ. Figure 1b, for example, depicts the structure of a single commensurate moiré cell for a t-BL with $\theta = 7.2°$. Figure 1c shows such a moiré pattern is clearly visible in the high-resolution annular dark-field scanning transmission electron microscopy (ADF-STEM) image of a twisted bilayer with a $\theta = 8.5°$ (see also Supporting Information Figure S1).

We construct t-BLs, such as the one shown in Figure 2a, by "stacking" single crystal flakes grown by chemical vapor deposition (details in the Supporting Information). Large (~10−100 μm) triangular crystals of monolayer MoS_2 are grown on silicon wafers with a 285 nm silicon oxide[24−26] overlayer. A single substrate is then broken in two, and a dry transfer procedure[11,24] is used to transfer the crystals from one-half of the sample to the other. Because there are hundreds of individual triangles on the substrate, each transfer creates dozens of overlapping triangles, resulting in the formation of t-BLs with a variety of twist angles. By optical investigations and atomic force microscopy, we find that the interface between the two layers is clean, aside from some bubbles or wrinkles trapped during the transfer procedure[11] (Supporting Information Figure S2). Because the triangles are not perfectly overlapped, we can also probe the individual monolayer crystals. These regions are indicated in Figure 2a, where the bottom layer is grown directly on the substrate and the top layer is transferred onto it.

We have previously shown that the lattice orientation of chemical vapor deposition (CVD)-grown triangles can be directly correlated to their morphology, allowing determination

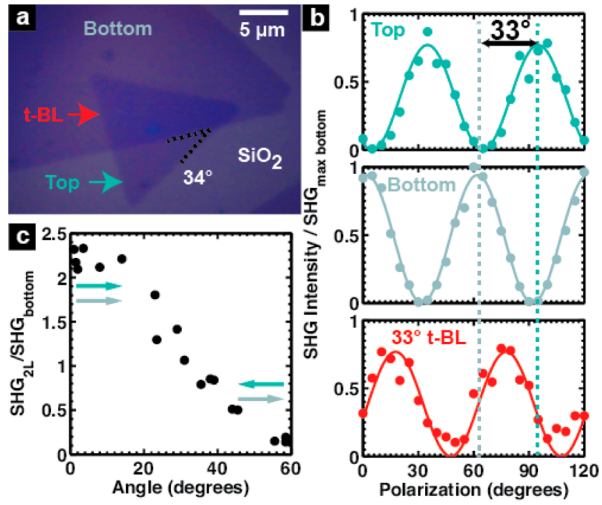

Figure 2. (a) Optical microscopy image of two overlapping CVD grown MoS_2 monolayer crystals, forming a twisted bilayer. The dashed lines indicate the different orientations of the triangle edges, which is a measure of the twist angle. (b) Second harmonic intensity as a function of angle of the polarization of the pump and detected radiation for the bottom (green), top (gray), and 33° twisted bilayer (red) shown in panel a. The solid lines are fits to the analytic model presented in the Supporting Information. (c) The measured ratio of the SH signal from the twisted bilayer to monolayer as a function of twist angles θ (black dots). The ratio is a maximum when the bilayers are aligned, and a minimum when the bilayers are antialigned.

of crystal orientation by optical microscopy.[24] We then extract the BL twist angle θ by measuring the relative orientations of edges of the two triangles. For example, the triangles shown in Figure 2a have molybdenum-terminated zigzag edges, and the bilayer has a twist angle of $\theta = 34°$. Using the same techniques as another work published during the final preparation of this manuscript,[27] we have also utilized optical second-harmonic generation (SHG) as a second probe of lattice orientation: For colinearly polarized pump and second-harmonic fields, the SH intensity is maximum for excitation along the armchair direction of a monolayer and vanishes for excitation along the zigzag direction.[27−30] By separately probing each region shown in Figure 2a, we directly compare SHG from the different layers (see Supporting Information for details and analysis). Figure 2b shows the SHG polarization dependence for the individual layers, as well as for the t-BL. From analysis of the orientational dependence of the SH response, we infer a twist angle of $\theta = 33°$, which is in close agreement with the

dx.doi.org/10.1021/nl501077m | Nano Lett. 2014, 14, 3869−3875

result obtained from analysis of the optical images of the triangular domains.

We found that the intensity of the SH emission from the bilayer is also a measure of twist angle. For example, the ratio of the maximum SH intensity of the bilayer to that of the bottom monolayer in Figure 2b is ∼0.8. Figure 2c shows the ratio of the bilayer to monolayer unpolarized SH intensity for t-BLs as a function of θ. The peak intensity of the SH signal in the t-BL varies continuously from its maximum for aligned (θ = 0°) samples down to nearly zero for antialigned (θ = 60°) samples. This behavior reflects the in-phase addition of the SH electric fields for the aligned case and the out-of-phase relation of the fields for the antialigned case. In the simple picture of two independent monolayers in free space, each with negligible optical absorption, we would expect to observe a SH intensity that is four times that of an individual monolayer for the aligned case and perfect destructive interference when the layers are antialigned. In our measurements, the antialigned samples are similar to previous measurements on exfoliated MoS_2,[28,29] where the 2H stacking leads to a centrosymmetric structure in even numbered stacks and a corresponding vanishing of the SH signal. However, the measured SH signal for the aligned samples is only ∼2 times that of the monolayer. The behavior reflects the optical absorption in the individual layers, the interlayer electronic coupling, and substrate effects.[27,24,25] The SHG technique enables optical quantification of the twist angle in any t-BL, even when the two component layers cannot be examined separately. It also confirms that the antialigned transferred BL samples are structurally similar to exfoliated bilayers and exhibit inversion symmetry.

To set the stage for our spectroscopic studies of twisted bilayers of MoS_2, let us recall the influence of layer thickness on the electronic structure and resulting optical transitions for 2H crystals of this material. The optical properties of MoS_2 (and related TMDs) near the onset of absorption are largely determined by a direct, dipole-allowed optical transition involving electronic states near the K-point of the Brillouin zone and an indirect optical transition to the Γ-point of the valence band requiring coupling to the phonons.[17] Spin−orbit interactions in the valence band split the direct transition into the A and B transitions near 1.85 and 2 eV, respectively, with the exact energies shifting with strain and doping.[31−35] In monolayers, the onset of the indirect transition is ∼200 meV higher in energy than the onset of the direct transition.[36] In the (antialigned) bilayer exfoliated from bulk 2H crystals, the indirect transition is downshifted to 1.5−1.6 eV.[17] The indirect transition is further downshifted to 1.29 eV in the bulk crystal.[17] Thus, monolayer MoS_2 is a direct-gap semiconductor, whereas multilayer MoS_2 samples are indirect-gap semiconductors. We note that electron−hole interactions in these materials, particularly in the monolayer, are strong and the optical transitions are actually excitonic in character, not simple band-to-band transitions.[35]

In Figure 3, we utilize optical spectroscopy to compare optical transitions in monolayers and t-BLs as a function of twist angle. Figure 3a shows photoluminescence spectra of t-BLs at various twist angles, as well as corresponding spectra of the bottom (as grown) and top (transferred) monolayers. Emission from the direct A transition is visible at 1.84−1.87 eV in all samples, but has much greater intensity in the monolayers (3−50×). The direct transition demonstrates only slight (few tens of meV) shifts in emission energy between the monolayers and t-BLs. In the t-BLs, however, a second peak is also observed

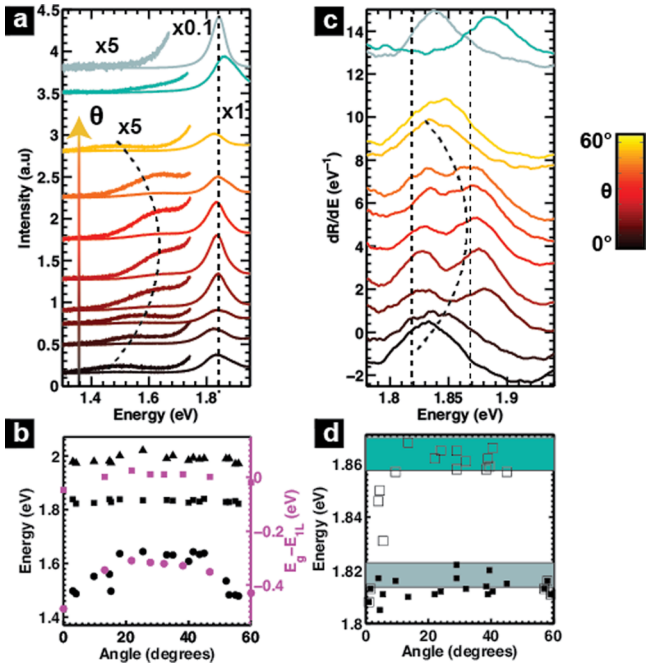

Figure 3. (a) Photoluminescence spectroscopy for 532 nm excitation for the bottom (as grown, gray line) and top (transferred, green line) monolayers and t-BLs at various twist angles θ. The spectra are offset for clarity and color-coded by θ as indicated with black corresponding to 0° and yellow to 60°. The black dashed lines highlight relevant tuning features. (b) Measured peak energies (black) versus θ for the indirect (circles), A (squares), and B (triangles) transitions. The magenta points indicate simulated transition energies for the t-BL structures of Figure 5b. The predicted peak position of the direct transition does not consider spin−orbit coupling and is normalized to the average position of the A and B transitions. (c) Linear reflection spectroscopy near the A transition for the top and bottom monolayers, as well as for t-BLs for many twist angles. The data are plotted as the derivative with respect to photon energy to highlight the relevant features. The A transition is split for bilayers at θ near 30° and merged for θ near 0° and 60°. (d) Extracted peak positions of the higher (open squares) and lower (filled squares) components of the A transition as a function of θ. The green and gray bars indicate the extracted peak positions for the bottom and top layers, respectively, with the width corresponding to the standard deviation of the different measurements.

at lower photon energies of 1.47−1.62 eV. These energies are similar to the 1.5−1.58 eV range for emission from the indirect transition in exfoliated bilayers. As with exfoliated bilayers, there is no indication of the lower-energy peak in absorption measurements, as is expected for a weak indirect transition. Similar behavior has also been observed in folded MoS_2 bilayers of unknown layer alignment in a preprint published during the preparation of this manuscript.[37] The presence of the lower-energy peak, the absence of any appreciable corresponding absorption, and the suppression of the photoluminescence from the A emission feature all strongly suggest that interlayer interaction causes t-BL MoS_2 to be an indirect-gap semiconductor even when the layers are not crystallographically aligned. This conclusion is further strongly supported by theoretical studies, as described below.

The dependence of the energy of the photoluminescence emission features on BL twist angle is presented in Figure 3b. The energy of the indirect transition is found to vary continuously and significantly with twist angle, increasing

dx.doi.org/10.1021/nl501077m | Nano Lett. 2014, 14, 3869−3875

from 1.47 eV for θ near 0° and 60° to 1.62 eV for θ near 30°. This second major finding demonstrates that the indirect transition in bilayer MoS_2 can be strongly tuned by interlayer twist angle. Because interlayer interaction reduces the energy of the indirect transition, it follows from the data that the effective interlayer interaction is maximized in the aligned/antialigned cases and is minimized near 30°.

In comparison with the indirect gap, the energy of the direct-gap A emission feature in all PL measurements varies little between the isolated single layer MoS_2 samples or with the twist angle in the bilayer samples. This general behavior is confirmed in reflection contrast measurements, which yield a response that approximates the absorption spectrum of the material. We present these experimental data in Figure 3c after taking a derivative with respect to photon energy to highlight the features and summarize the measured peak energies in Figure 3d. On the energy scale of tens of millielectronvolts, we observe a small and complex variation of the A transition with twist angle, which we will discuss after building a theoretical framework below. We have also examined the characteristic tuning of the B and C transitions with twist angle and present the results in Supporting Information Figure S3.

In addition to the tuning of the optical transitions with twist angle, we also observe distinct tuning of the phonon modes. Figure 4 shows Raman spectra and corresponding extracted peak positions of the in-plane E_{2g} (~384 cm^{-1}) phonon mode (Figure 4a,b) and out-of-plane A_{1g} (~403 cm^{-1}) phonon mode (Figure 4c,d) of the monolayers and t-BLs at various twist angles. As for the optical transitions, there are small spectral shifts between the bottom and top isolated monolayers for the E_{2g} mode, although the A_{1g} mode shows no significant shift for the two monolayers. With respect to the bilayer twist angle, we observe in our measurements opposite tuning behavior for the E_{2g} and A_{1g} Raman modes. For the E_{2g} mode, there is a symmetrical upshift of 1 cm^{-1} around 30° compared to either 0 or 60°. The A_{1g} mode shows a similar behavior but with downshift of 1.5 cm^{-1} near 30°. Below we provide a theoretical framework for explaining these trends.

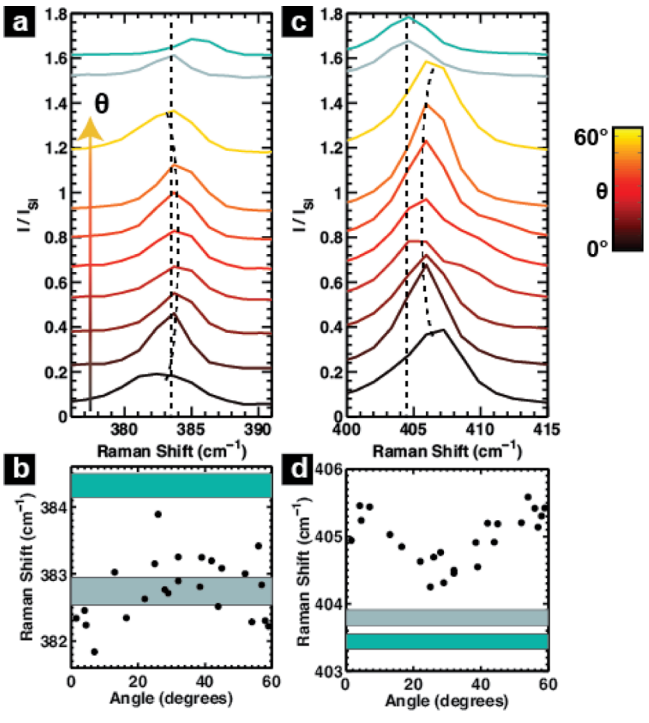

Figure 4. (a) Tuning of the Raman E_{2g} mode with twist angle θ and (b) extracted peak positions (black points). (c) Tuning of the Raman A_{1g} mode with θ and (d) the extracted peak positions (black points). The spectra are offset for clarity and color-coded by twist angle, as indicated, with black corresponding with 0° and yellow corresponding with 60°. Black dashed lines highlight relevant tuning features. The green and gray bars indicate the standard deviation in the extracted peak positions for the bottom and top layers, respectively.

In order to explain the observed tuning of optical transitions, we have developed a simple model attributing shifts in the energy levels in the electronic structure primarily to changes in interlayer separation as a function of twist angle. Intuitively, the origin of this change is easy to understand and is demonstrated graphically in Figure 5a. The MoS_2 monolayer is corrugated on the atomic scale, and the interlayer separation in the bilayer depends on the alignment of the atoms in the two layers. In the one extreme, as shown in Figure 5a, the sulfur atoms are vertically aligned, leading to maximum layer separation. At the other extreme, as we see for 0 and 60° twist angle in Figure 1a, the bilayer separation will be a minimum when the inner sulfur

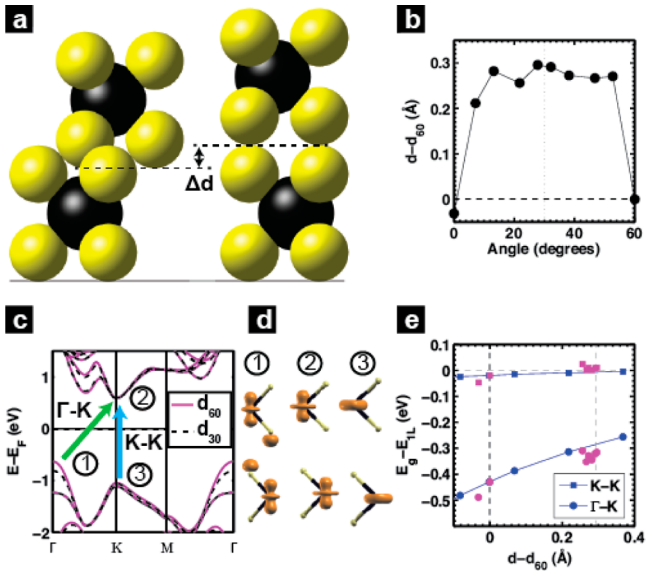

Figure 5. (a) The surface of a MoS_2 monolayer is corrugated because the sulfur atoms (yellow) project out of the plane. As a result, the interlayer separation depends on the relative position of the sulfur atoms in the two layers. (b) Bilayer separation as a function of twist angle θ relative to the 60° separation of d_0 = 6.23 Å determined from dispersion-corrected density functional theory calculations (DFT). The bilayer separation for intermediate θ is greater than for the crystallographic orientations (0 and 60°). (c) Electronic structures of a 60° bilayer system with separations corresponding to 60° (solid lines) and 30° (broken lines), highlighting the impact of layer separation. The energy of the valence band at the Γ-point varies strongly with the separation. (d) The partial charge density of states corresponding to, the valence band at the Γ-point (State 1), the conduction band at the K-point (State 2), and the valence band at the K-point (State 3). Only State 1 involves inner sulfur atoms, explaining why the indirect transition is affected by twist angle. (e) The change of the direct (K–K) and indirect (Γ–K) transitions as a function of separation for the 60° bilayer system (blue) and the corresponding values from the fully relaxed, rotated systems (magenta). While the direct transition exhibits almost no variation with separation, the indirect transition shows a strong dependence.

dx.doi.org/10.1021/nl501077m | Nano Lett. 2014, 14, 3869–3875

atoms in the two layers are staggered with the molybdenum atoms in one layer being vertically aligned with the sulfur atoms in the other. Any interlayer translation, twist, or strain is expected to lead to an effective layer separation lying between these two extremes.

We quantify the expected changes in layer separation due to twist and translation using dispersion-force corrected density functional theory (DFT-D2, see Supporting Information)[38−42] applied to a series of t-BLs at angles with commensurate unit cells (Supporting Information Figures S4 and S5 for details, including a comparison to a simpler, hard-sphere model, and a discussion of interlayer corrugation).

Figure 5b shows the predicted average bilayer separation as a function of twist angle. The in-plane translation between layers is picked to give the minimum separation (Supporting Information). The DFT-D2 calculations predict a d_{60} = 6.23 Å separation for the crystallographically oriented 2H phase (60° or antialigned), compared with the experimentally measured 6.15 Å for bulk MoS_2.[43] The separation is increased for all twist angles up to a maximum value of d_{30} = 6.52 Å at 30°, representing an increase of 0.29 Å or 5%. This increase in separation is about half the predicted 0.59 Å or 11% increase in separation for the aligned sulfur geometry. These shifts represent large changes compared with those typically achievable through temperature or strain. A steep increase in interlayer separation is obtained for twist angles near 0 and 60°. The functional dependence of the bilayer separation for such angles (requiring simulations with very large unit cells) will be examined in future studies.

In order to understand the impact of changes in interlayer spacing, we show in Figure 5c the band structure for a 2H bilayer at layer separations of d_{60} = 6.23 Å (purple) and d_{30} = 6.52 Å (black dashed), corresponding to the range of separation seen in the twisted system (see also Supporting Information Figure S5). While there is almost no change in the energy of the states near K that determine the onset of the A transitions, the highest occupied state near Γ is substantially downshifted for larger separation. As a result, the onset of the Γ−K indirect electronic band gap and optical transition increased by 147 meV. In these calculations, we focus only on shifts in the transition energies arising from changes in structure. The predicted K−K transition of 1.66 eV is less than the experimentally measured value of 1.86 eV due to systematic limitations in DFT calculations. While more accurate results can be obtained using many-body perturbation theory methods,[44] previous studies have shown that the calculated shifts in band structure predicted by DFT, for example, with pressure, are accurate.[45]

The strong tuning in the Γ−K transition with interlayer separation, as well as the much smaller tuning of the K−K transition, have an origin similar to that previously identified for tuning with number of layers in the crystallographic structures.[17,18] Figure 5d shows the partial charge density of the three band states numbered in Figure 5c. The valence (State 3) and conduction (State 2) band states related to the direct transition at the K-point involve Mo-d states that are localized within the two layers, while the valence state at the Γ-point (State 1) has appreciable p_z content of the S atoms between layers, as well as Mo-d_z^2 character. The overlap of the S-p_z orbitals and the resulting band energy of State 1 depend strongly on the interlayer separation. Thus, the interlayer electronic coupling is mainly defined by the orbital overlap of the inner sulfur atoms.

The results in Figure 5c highlight the impact of interlayer spacing, but retain the crystallographic alignment of the layers. In the twisted bilayer, the alignment of the S atoms systematically varies across the moiré pattern. We consider the impact of this by analyzing the optical transitions allowed for the commensurate t-BLs described above with the equilibrium spacing separations in Figure 5b (Supporting Information Figure S6). Figure 5e compares the extracted transitions energies versus layer separation for the case where the layer spacing of aligned layers is changed (as in Figure 5c) and for the cases of fully relaxed, t-BLs. In both cases, the K−K direct band transition exhibits small changes, while the Γ−K indirect band transition follows a nearly linear upward trend with increased separation. Moreover, the indirect band transition of both the aligned and twisted cases are quantitatively very similar. Finally, we considered t-BLs at fixed layer spacing to find that twist without change in separation has a small contribution compared with interlayer spacing (Supporting Information Figure S7). Overall, we conclude that average layer separation is the key parameter controlling interlayer coupling on the valence band state at Γ and hence for the indirect band gap (see also, Supporting Information Figure S7).

Returning to Figure 3b, the experimentally determined energies of the direct and indirect transitions (black points) are accompanied by theoretical values obtained for the fully relaxed t-BLs (magenta points). We obtain excellent agreement with the data, which confirms that the lower peak indeed corresponds to an indirect transition. In practice, the theory is performed for the special case of commensurate t-BL structures while the measured results correspond to more common incommensurate structures. However, it is still possible to compare these results by following the logic previously applied to twisted graphene bilayers.[13,46,47] In this model, it is helpful to think of the twisted bilayer as two separate monolayers with states labeled according to their own Brillouin zone. As these two layers are brought together to form the bilayer, they couple wherever there is band edge overlap. At the K-point, the bands will only overlap when the t-BL forms a commensurate structure and transitions map to a common K-point in the reduced Brillouin zone for the superstructure. Even so, due to the lack of orbital overlap between the layers (Figure 5d), the variation in the direct transition energy is small. Meanwhile, in incommensurate structures, the K-points for the two layers will be separated in momentum space and the effective interaction will be even weaker than in commensurate structures. In contrast, states at the Γ-point have zero momentum, which is the axis of rotation in a twisted structure. As a result, valence band edge states at Γ from each layer will be resonant with each other regardless of twist angle and the magnitude of the interlayer coupling will be similar to the commensurate t-BL structures. Thus, the calculated transitions for commensurate structures should robustly apply to the measured incommensurate structures.

Our analysis is seen to predict the strong tuning of the indirect transition with twist angle and the lack of significant tuning in the direct transition in terms of the changing interlayer separation and the character of the wave functions in different parts of the Brillouin zone. We do, however, also observe weak tuning in the direct transition energy and Raman mode frequencies with twist angle, as presented above. While we do not have detailed quantitative explanation of the results,

dx.doi.org/10.1021/nl501077m | Nano Lett. 2014, 14, 3869−3875

the trend for both these responses is consistent with the general character of the interlayer interactions discussed above.

First, we note that the bottom and top layers are not precisely identical as assumed in the calculations and the simple picture: compared with the as-grown monolayer, the transferred monolayer on oxide displays a small 40 meV upshift in the A transition, a 1.5 cm^{-1} upshift in the E_{2g} mode, and a 0.25 cm^{-1} upshift in the A_{1g} mode. By comparing to previous work quantifying the effects of strain[31,32] and doping[33−35] on transition energies, we associate these shifts with a decrease of strain in the top layer induced by the transfer process (details in Supporting Information). This strain should not significantly affect the fundamental conclusions of the simple model but adds complexity to interpreting the higher order tuning.

For example, in the reflection contrast measurements in Figure 3c, t-BLs with twist angles away from 0 and 60°, the peaks in the bilayer samples closely resemble a superposition of the two (offset) monolayer peaks. For angles near 0 and 60°, however, the bilayer exhibits a single peak near the energy of the lower feature in the isolated layers. This data strongly suggests that the interlayer interaction is maximum when the two layers are aligned or antialigned. In the model presented above, we predict very little dependence of the K−K transition on interlayer separation. However, higher order interaction of the layers will be strongest when the dispersion relations in the individual layers overlap in both momentum and energy. Also, how interlayer strain will distribute will depend on the twist angle.[12] Either way, we expect the strongest interaction of states near the K-point when the layers are aligned or antialigned, as observed in the data.

Similarly, the Raman modes in MoS_2 are sensitive to layer interactions. To put the results in context, as the layer thickness increases, the E_{2g} mode downshifts and the A_{1g} upshifts.[19] Exfoliated monolayers exhibit a difference in mode frequency of $\Delta\omega$ = 19 cm^{-1}, which increases to 20.5 cm^{-1} in bilayers and up to 25.2 cm^{-1} in the bulk. As seen in Figure 4, when the t-BLs move closer together with twist angle, the E_{2g} mode shifts down and the A_{1g} mode shifts up. The tuning suggests that the effective layer interaction is maximum near 0 and 60° and minimum near 30°, as expected based on the interlayer separation of the MoS_2 monolayers.

Despite this qualitative understanding of the observed trends, a more precise description of the weak tuning in the direct band transitions and Raman modes is unavailable at present. Extrinsic perturbations such as interlayer strain or doping induced by the transfer process,[31−35] or intrinsic perturbations such as breaking of the band degeneracy induced by many body interactions should all impact the observed behavior (more in Supporting Information). So far, simulations exploring these higher-order tuning effects have been inconclusive. Nonetheless, the observed trends are robust and motivate the development of more advanced models to account for both intrinsic and extrinsic effects.

Taken together, we have experimentally and theoretically shown that many optical and electronic properties in bilayer MoS_2 are extremely sensitive to the relative orientation of the layers. In particular, the orbital energy for the valence band edge state at the Γ point is most sensitive to interlayer interactions due to the overlap in the valence band orbitals between the layers regardless of twist angle, while the energies of the band edge states at the K-point are relatively insensitive. Moreover, we can tune these interactions by tuning the interlayer distance via twist. This important result has important implications not just for understanding other TMD bilayer systems but also heterojunction interfaces of disparate TMDs. Using the same reasoning applied to the homojunction, heterojunctions of TMDs should still have significant perturbations at the gamma point, which can strongly affect both material and device properties. Given the recent surge in interest in TMD heterojunctions,[20−23] it is clear that understanding and controlling interlayer interactions through layer orientation is going to be a crucial variable that must be taken into account in device design but also provides a new route toward control of the properties of atomically thin sheets.

■ ASSOCIATED CONTENT

Supporting Information

Information on the growth of the CVD MoS_2 monolayers and construction of the twisted bilayers, along with details on the experimental measurements and numerical methods, and Figures S1−S7. This material is available free of charge via the Internet at http://pubs.acs.org.

■ AUTHOR INFORMATION

Corresponding Author

*E-mail: av2466@columbia.edu.

Author Contributions

A.M.v.d.Z conceived the idea and supervised all aspects of the project. MoS_2 growth was carried out by D.A.C. under supervision from J.C.H. The twisted bilayers were fabricated by A.M.v.d.Z with assistance from L.W. and F.Z. Transmission electron microscopy was carried out by P.Y.H. with supervision by D.A.M. Optical spectroscopy and data analysis were carried out by A.M.v.d.Z., A.C., Y.Y., and X.Z. under supervision by T.F.H. Electronic structure calculations were carried out by J.K and T.C.B. under supervision by D.R.R. and M.S.H. A.M.v.d.Z., J.K., A.C., M.S.H., T.F.H., and J.C.H. wrote the paper.

Notes

The authors declare no competing financial interest.

(J.K.) On leave from Institute for Materials Science and Max Bergmann Center of Biomaterials, TU Dresden, 01062 Dresden, Germany.

■ ACKNOWLEDGMENTS

Overall project coordination, sample growth, and optical characterization were supported as part of the Center for Re-Defining Photovoltaic Efficiency Through Molecular-Scale Control, an Energy Frontier Research Center funded by the U.S. Department of Energy (DOE), Office of Science, Office of Basic Energy Sciences under Award DE-SC0001085. A.M.v.d.Z and J.K. were supported by the EFRC as research fellow and postdoctoral researcher, respectively. A.C. was supported by the Alexander von Humboldt Foundation through the Feodor-Lynen fellowship program. Electron microscopy was performed at and supported by the Cornell Center for Materials Research, a National Science Foundation MRSEC (NSF DMR-1120296). Computations were performed at the Center for Information Services and High Performance Computing (ZIH) of the TU Dresden. P.Y.H. was supported under NSF Graduate Research Fellowship Grant DGE-0707428. D.A.C. was supported by a Columbia University Presidential fellowship and a GEM Ph.D. Fellowship sponsored by the Center for Functional Nanomaterials at Brookhaven National Lab. Part of this work was carried out at the Center for Functional Nanomaterials, Brookhaven National Laboratory, which is supported by the

U.S. Department of Energy, Office of Basic Energy Sciences, under contract no. DEAC02-98CH10886. The authors thank Sasha Gondarenko, Yilei Li, Philip Kim, Gwan Hyoung Lee, and Chul-Ho Lee for helpful discussions.

REFERENCES

(1) Radisavljevic, B.; Radenovic, A.; Brivio, J.; Giacometti, V.; Kis, A. *Nat. Nanotechnol.* **2011**, *6* (3), 147−150.
(2) Wang, H.; Yu, L.; Lee, Y.-H.; Shi, Y.; Hsu, A.; Chin, M. L.; Li, L.-J.; Dubey, M.; Kong, J.; Palacios, T. *Nano Lett.* **2012**, *12* (9), 4674−4680.
(3) Lee, G.-H.; Yu, Y.-J.; Cui, X.; Petrone, N.; Lee, C.-H.; Choi, M. S.; Lee, D.-Y.; Lee, C.; Yoo, W. J.; Watanabe, K.; Taniguchi, T.; Nuckolls, C.; Kim, P.; Hone, J. *ACS Nano* **2013**, *7* (9), 7931−7936.
(4) Georgiou, T.; Jalil, R.; Belle, B. D.; Britnell, L.; Gorbachev, R. V.; Morozov, S. V.; Kim, Y.-J.; Gholinia, A.; Haigh, S. J.; Makarovsky, O.; Eaves, L.; Ponomarenko, L. A.; Geim, A. K.; Novoselov, K. S.; Mishchenko, A. *Nat. Nanotechnol.* **2013**, *8* (2), 100−103.
(5) Sup Choi, M.; Lee, G.-H.; Yu, Y.-J.; Lee, D.-Y.; Hwan Lee, S.; Kim, P.; Hone, J.; Jong Yoo, W. *Nat. Commun.* **2013**, *4*, 1624.
(6) Radisavljevic, B.; Whitwick, M. B.; Kis, A. *ACS Nano* **2011**, *5* (12), 9934−9938.
(7) Britnell, L.; Gorbachev, R. V.; Jalil, R.; Belle, B. D.; Schedin, F.; Mishchenko, A.; Georgiou, T.; Katsnelson, M. I.; Eaves, L.; Morozov, S. V.; Peres, N. M. R.; Leist, J.; Geim, A. K.; Novoselov, K. S.; Ponomarenko, L. A. *Science* **2012**, *335* (6071), 947−950.
(8) Lee, H. S.; Min, S.-W.; Chang, Y.-G.; Park, M. K.; Nam, T.; Kim, H.; Kim, J. H.; Ryu, S.; Im, S. *Nano Lett.* **2012**, *12* (7), 3695−3700.
(9) Fontana, M.; Deppe, T.; Boyd, A. K.; Rinzan, M.; Liu, A. Y.; Paranjape, M.; Barbara, P. *Sci. Rep.* **2013**, *3*, 1634.
(10) Terrones, H.; López-Urías, F.; Terrones, M. *Sci. Rep.* **2013**, *3*, 1549.
(11) Dean, C. R.; Young, A. F.; Meric, I.; Lee, C.; Wang, L.; Sorgenfrei, S.; Watanabe, K.; Taniguchi, T.; Kim, P.; Shepard, K. L.; Hone, J. *Nat. Nanotechnol.* **2010**, *5* (10), 722−726.
(12) Alden, J. S.; Tsen, A. W.; Huang, P. Y.; Hovden, R.; Brown, L.; Park, J.; Muller, D. A.; McEuen, P. L. *Proc. Natl. Acad. Sci. U.S.A.* **2013**, *110* (28), 11256−11260.
(13) Havener, R. W.; Zhuang, H.; Brown, L.; Hennig, R. G.; Park, J. *Nano Lett.* **2012**, *12* (6), 3162−3167.
(14) Li, G.; Luican, A.; Andrei, E. Y. *Phys. Rev. Lett.* **2009**, *102* (17), 176804.
(15) Dean, C. R.; Wang, L.; Maher, P.; Forsythe, C.; Ghahari, F.; Gao, Y.; Katoch, J.; Ishigami, M.; Moon, P.; Koshino, M.; Taniguchi, T.; Watanabe, K.; Shepard, K. L.; Hone, J.; Kim, P. *Nature* **2013**, *497* (7451), 598−602.
(16) Hunt, B.; Sanchez-Yamagishi, J. D.; Young, A. F.; Yankowitz, M.; LeRoy, B. J.; Watanabe, K.; Taniguchi, T.; Moon, P.; Koshino, M.; Jarillo-Herrero, P.; Ashoori, R. C. *Science* **2013**, *340* (6139), 1427−1430.
(17) Mak, K. F.; Lee, C.; Hone, J.; Shan, J.; Heinz, T. F. *Phys. Rev. Lett.* **2010**, *105* (13), 136805.
(18) Splendiani, A.; Sun, L.; Zhang, Y.; Li, T.; Kim, J.; Chim, C.-Y.; Galli, G.; Wang, F. *Nano Lett.* **2010**, *10* (4), 1271−1275.
(19) Lee, C.; Yan, H.; Brus, L. E.; Heinz, T. F.; Hone, J.; Ryu, S. *ACS Nano* **2010**, *4* (5), 2695−2700.
(20) Rivera, P.; Schaibley, J. R.; Jones, A. M.; Ross, J. S.; Wu, S.; Aivazian, G.; Klement, P.; Ghimire, N. J.; Yan, J.; Mandrus, D. G.; Yao, W.; Xu, X. arxiv preprint arXiv.1403.4985 2014 (accessed May 19, 2014).
(21) Lee, C.-H.; Lee, G.-H.; van der Zande, A. M.; Chen, W.; Li, Y.; Han, M.; Cui, X.; Arefe, G.; Nuckolls, C.; Heinz, T. F.; Hone, J.; Kim, P. arXiv preprint arXiv:1403.3062 2014 (accessed May 19, 2014).
(22) Furchi, M. M.; Pospischil, A.; Libisch, F.; Burgdörfer, J.; Mueller, T. arXiv preprint arXiv:1403.2652 2014 (accessed May 19, 2014).
(23) Fang, H.; Battaglia, C.; Carraro, C.; Nemsak, S.; Ozdol, B.; Kang, J. S.; Bechtel, H. A.; Desai, S. B.; Kronast, F.; Unal, A. A.; Conti, G.; Conlon, C.; Palsson, G. K.; Martin, M. C.; Minor, A. M.; Fadley, C. S.; Yablonovitch, E.; Maboudian, R.; Javey, A. *Proc. Natl. Acad. Sci. U.S.A.* **2014**, *111* (17), 6198−6202.
(24) van der Zande, A. M.; Huang, P. Y.; Chenet, D. A.; Berkelbach, T. C.; You, Y.; Lee, G.-H.; Heinz, T. F.; Reichman, D. R.; Muller, D. A.; Hone, J. C. *Nat. Mater.* **2013**, *12* (6), 554−561.
(25) Zhan, Y. J.; Liu, Z.; Najmaei, S.; Ajayan, P. M.; Lou, J. *Small* **2012**, *8* (7), 966−971.
(26) Najmaei, S.; Liu, Z.; Zhou, W.; Zou, X.; Shi, G.; Lei, S.; Yakobson, B. I.; Idrobo, J.-C.; Ajayan, P. M.; Lou, J. *Nat. Mater.* **2013**, *12* (8), 754−759.
(27) Hsu, W.-T.; Zhao, Z.-A.; Li, L.-J.; Chen, C.-H.; Chiu, M.-H.; Chang, P.-S.; Chou, Y.-C.; Chang, W.-H. *ACS Nano* **2014**, *8* (3), 2951−2958.
(28) Li, Y.; Rao, Y.; Mak, K. F.; You, Y.; Wang, S.; Dean, C. R.; Heinz, T. F. *Nano Lett.* **2013**, *13* (7), 3329−3333.
(29) Malard, L. M.; Alencar, T. V.; Barboza, A. P. M.; Mak, K. F.; de Paula, A. M. *Phys. Rev. B* **2013**, *87* (20), 201401.
(30) Kim, C.-J.; Brown, L.; Graham, M. W.; Hovden, R.; Havener, R. W.; McEuen, P. L.; Muller, D. A.; Park, J. *Nano Lett.* **2013**, *13* (11), 5660−5665.
(31) Conley, H. J.; Wang, B.; Ziegler, J. I.; Haglund, R. F.; Pantelides, S. T.; Bolotin, K. I. *Nano Lett.* **2013**, *13* (8), 3626−3630.
(32) He, K.; Poole, C.; Mak, K. F.; Shan, J. *Nano Lett.* **2013**, *13* (6), 2931−2936.
(33) Chakraborty, B.; Bera, A.; Muthu, D. V. S.; Bhowmick, S.; Waghmare, U. V.; Sood, A. K. *Phys. Rev. B* **2012**, *85*, 161101.
(34) Ross, J. S.; Wu, S.; Yu, H.; Ghimire, N. J.; Jones, A. M.; Aivazian, G.; Yan, J.; Mandrus, D. G.; Xiao, D.; Yao, W.; Xu, X. *Nat. Commun.* **2013**, *4*, 1474.
(35) Mak, K. F.; He, K.; Lee, C.; Lee, G. H.; Hone, J.; Heinz, T. F.; Shan, J. *Nat. Mater.* **2012**, *12* (3), 207−211.
(36) Jin, W.; Yeh, P.-C.; Zaki, N.; Zhang, D.; Sadowski, J. T.; Al-Mahboob, A.; van der Zande, A. M.; Chenet, D. A.; Dadap, J. I.; Herman, I. P.; Sutter, P.; Hone, J.; Osgood, R. M. *Phys. Rev. Lett.* **2013**, *111* (10), 106801.
(37) Castellanos-Gomez, A.; van der Zant, H. S.; Steele, G. A. *Nano Res.* **2013**, *7* (4), 1−7.
(38) Perdew, J. P.; Burke, K.; Ernzerhof, M. *Phys. Rev. Lett.* **1996**, *77* (18), 3865−3868.
(39) Grimme, S. *J. Comput. Chem.* **2006**, *27* (15), 1787−1799.
(40) Blöchl, P. E. *Phys. Rev. B* **1994**, *50* (24), 17953−17979.
(41) Kresse, G.; Furthmüller, J. *Phys. Rev. B* **1996**, *54* (16), 11169−11186.
(42) Kresse, G.; Furthmüller, J. *Comput. Mater. Sci.* **1996**, *6* (1), 15−50.
(43) Schonfeld, B.; Huang, J. J.; Moss, S. C. *Acta Crystallogr., Sect, B* **1983**, *39* (4), 404−407.
(44) Onida, G.; Reining, L.; Rubio, A. *Rev. Mod. Phys.* **2002**, *74* (2), 601−659.
(45) Zhu, X.; Fahy, S.; Louie, S. G. *Phys. Rev. B* **1989**, *39* (11), 7840−7847.
(46) Shallcross, S.; Sharma, S.; Kandelaki, E.; Pankratov, O. A. *Phys. Rev. B* **2010**, *81* (16), 165105.
(47) Shallcross, S.; Sharma, S.; Pankratov, O. A. *Phys. Rev. Lett.* **2008**, *101* (5), 056803.